Prediction of solid recirculation rate and solid volume fraction in an ICFB

***Ravi Gujjula[1], Narasimha Mangadoddy[1].**

[1]Department of Chemical Engineering, Indian Institute of Technology Hyderabad, Ordnance Factory Estate, 502205, Andhra Pradesh, India.

*Corresponding author: narasimha@IITH.AC.IN

Abstract

This paper presents a numerical study of gas and solid flow in an internally circulating fluidized bed (ICFB). The gas and solid hydrodynamics have been simulated by using two-fluid model. 2D & 3D geometry was used to represent key parts of a laboratory ICFB. In ICFB, the two-fluid Eulerian model with kinetic theory of granular flow option and the various drag laws used to predict the hydrodynamic behavior of ICFB. The simulation results by four drag laws show that the Gidaspow and Arastoopour drag models predict the fluidization dynamics in terms of flow patterns, void fractions and axial velocity fields were compared with experimental data. The effect of superficial gas velocity, presence of draft tube on solid hold-up distribution, solid circulation pattern, and variations in gas bypassing fraction for the 3D ICFB investigated through CFD simulations**.** The mechanism governing the solid circulation in an ICFB has been explained based on gas and solid dynamics obtained from the simulations. Predicted total granular temperature distributions in the draft tube and annular zones qualitatively agree with experimental data. The total granular temperature tends to increase with increasing solids concentrations and decrease with an increase of solids concentration.

Key words: ICFB; Two fluid model; Solid recirculation rate; Gas solid granular flow; Drag law models; Fluidization, Hydrodynamics.

*Corresponding author: ch09p002@iith.ac.in, Fax: +91 4023016032

1. Introduction

Gas-solid fluidization by conventional circulating fluidized beds (CFB) are common in various industrial operations such as coal combustion and gasification, incineration of municipal solid waste, catalyst regeneration, thermal cracking and drying (Yang et al., 2008; Kim et al., 1997,2000; Burugupalli 1988). They require very long tall column as a solids raiser and accompanying additional external circulation of solids through a cyclone. In order to avoid external circulation accessories, a compact internally circulating fluidized bed (ICFB) is developed, which is a modified spouted fluidized bed with a draft tube inside the column to avoid problem of gas bypassing. An ICFB is having a centrally located draft tube that divides the bed into two or more sections and thus promotes solid circulation within a single vessel (Kim et al., 1997, 2000; Burugupalli, 1988; Yang & Keairns, 1978). This ICFB reactor has many advantages such as its compact size and the annular section act as heat sink because riser is located inside the vessel (Jeon & Kim, 2010). The ICFB reduces the height of conventional CFB riser and construction cost, solves the problems of CFB, makes highly efficient and low pollution combustion for a wide range of fuels. In ICFB, the draft tube (or riser) was fixed directly to the gas distributor of the riser section.

In recent years due to advances in high performance computers and numerical algorithms, the computational fluid dynamics (CFD) technique is become a fundamental element of research in simulating gas–solid multiphase flow systems (Mujumdar, & Wu, 2008). Thus many researchers have put considerable effort in validating the CFD models in order to achieve fundamental and accurate model for these systems. One of the difficulties to validate CFD models using experimental measurements is the computational effort needed to perform three-dimensional (3D) simulations of dynamic behavior of industrial scale fluidized beds. Several drag models have been developed to calculate the inter-phase momentum exchange in fluidized bed, such as the Wen and Yu, Syamlal & O'Brien and Gidaspow drag models (Wen & Yu, 1966; Syamlal, & O'Brien, 1989; Gidaspow, 1994). The effect of various drag models on hydrodynamics behavior of gas–solid fluidized beds was also compared by (Van Wachem et al., 2001). They found that the expression suggested by Syamlal–O'Brien (Syamlal, & O'Brien, 1989) model under predicts the pressure drop, bed expansion and bubble diameter compared to the experimental data. The work reported in this paper aimed at the development of a CFD-model for the hydrodynamics of 3D- ICFB reactor. With the help of this CFD model the instantaneous and the time-averaged profiles of pressure drop and volume fractions within the draft tube and the annulus section of ICFB calculated. Further, the flow fields, i.e. volume fractions and velocity distributions predicted for different size particles in the range of 86 μm-250 μm. Additionally 2D-ICFB CFD simulations run to validate the CFD model predictions. These predictions are then compared to the experimental data of Ahuja, & Patwardhan, (2008).

2. Methodology

2. 1. Eulerian–Eulerian model equations for gas–solid flow with KTGF

The partial differential TFM equations for explaining particle and fluid flows in the fluidized bed (Patankar, 1980) are adopted for the ICFB. The continuity equation in the absence of mass transfer between phases is give for each phase as follows

$$\frac{\partial}{\partial t}(\varepsilon_g \rho_g) + \nabla.(\varepsilon_g \rho_g v_g) = 0 \tag{1}$$

$$\frac{\partial}{\partial t}(\varepsilon_s \rho_s) + \nabla.(\varepsilon_s \rho_s v_s) = 0 \tag{2}$$

$$\varepsilon_g + \varepsilon_s = 1 \tag{3}$$

Momentum conservation equations

$$\frac{\partial}{\partial t}(\varepsilon_g \rho_g \upsilon_g) + \nabla.(\varepsilon_g \rho_g \upsilon_g \upsilon_g) = \nabla.\tau_g + \varepsilon_g \rho_g g - \varepsilon_g \nabla P + \beta(\upsilon_g - \upsilon_s) \tag{4}$$

$$\frac{\partial}{\partial t}(\varepsilon_s \rho_s \upsilon_s) + \nabla.(\varepsilon_s \rho_s \upsilon_s \upsilon_s) = \nabla.\tau_s + \varepsilon_s \rho_s g - \nabla P_s - \varepsilon_s \nabla P + \beta(\upsilon_g - \upsilon_s) \tag{5}$$

The solid pressure is composed of a kinetic term and a second term due to particle collisions as follows (Luna et al., 1984)

$$P_s = \varepsilon_s \rho_s \Theta_s + 2\rho_s(1+e_s)\varepsilon_s^2 g_o(\varepsilon_s)\Theta_s \tag{6}$$

$$\tau_s = \varepsilon_s \mu_s \left(\nabla \upsilon_s + (\nabla \upsilon_s)^T\right) + \varepsilon_s(\lambda_s - \frac{2}{3}\mu_s)(\nabla.\upsilon_s).I \tag{7}$$

$$\tau_g = \varepsilon_g \mu_g \left(\nabla \upsilon_g + (\nabla \upsilon_g)^T\right) - \frac{2}{3}\varepsilon_g \mu_g (\nabla.\upsilon_g).I \tag{8}$$

$$\lambda_s = \frac{4}{3}\varepsilon_s \rho_s d_p g_0(\varepsilon_s)(1+e_s)\sqrt{\frac{\Theta_s}{\pi}} \tag{9}$$

2.2. Drag models

The mathematical formulations of the four drag models that have been used in this work are shown below.

Gidaspow's drag model (1994).

$$\beta_{Wen-Yu} = \frac{3C_D \varepsilon_s \varepsilon_g \rho_g |\upsilon_g - \upsilon_s|}{4d_p}\varepsilon_g^{-2.65}, \qquad \varepsilon_g \geq 0.8 \tag{10}$$

$$\beta_{Ergun} = 150\frac{\varepsilon_s^2 \mu_g}{\varepsilon_g d_p^2} + 1.75\frac{\varepsilon_s \mu_g |\upsilon_g - \upsilon_s|}{d_p}, \qquad \varepsilon_g < 0.8 \tag{11}$$

$$C_D = \begin{cases} \frac{24}{\mathrm{Re}_p}[1+0.15(\mathrm{Re}_p)^{0.687}], & \mathrm{Re_p} < 1000 \\ 0.44 \quad , & \mathrm{Re_p} > 1000 \end{cases} \tag{12}$$

$$\mathrm{Re}_p = \frac{\varepsilon_g \rho_g d_p |\upsilon_g - \upsilon_s|}{\mu_g} \quad , \text{ Particle Reynolds Number} \tag{13}$$

Arastoopour's drag model (1990)

$$\beta_{gs} = \left(\frac{17.3}{\mathrm{Re}_p} + 0.336\right)\frac{\rho_g |\upsilon_g - \upsilon_s|}{d_p}(1-\varepsilon_g)\varepsilon_g^{-2.8} \tag{14}$$

Syamlal–O'Brien (1989) is expressed as

$$\beta_{gs} = \frac{3}{4}\frac{\varepsilon_g \varepsilon_s \rho_g}{v_{rs}^2 d_p} C_D\left(\frac{\mathrm{Re}_p}{v_{rs}}\right)|\upsilon_g - \upsilon_s| \tag{15}$$

$$C_D = \left(0.63 + \frac{4.8}{\sqrt{\mathrm{Re}_p / v_{rs}}}\right)^2 \tag{16}$$

$$\mathrm{Re}_p = \frac{\rho_g d_p |\upsilon_g - \upsilon_s|}{\mu_g} \tag{17}$$

$$v_{rs} = 0.5\left[A - 0.06\mathrm{Re}_p + \sqrt{(0.06\mathrm{Re}_p)^2 + 0.12\mathrm{Re}_p(2B-A) + A^2}\right] \tag{18}$$

$$A = \varepsilon_g^{4.14}, B = \begin{cases} 0.8\varepsilon_g^{1.28} & for\ \varepsilon_g \le 0.85 \\ \varepsilon_g^{2.65} & for\ \varepsilon_g \ge 0.85 \end{cases} \tag{19}$$

Fig.1. shows the relationship between the fluid-solid phase exchange coefficient, which is estimated for the available drag models in the literature as a function of solids volume fraction. For the various drag models at fixed slip velocity of 0.5 m/s and for the 86 µm, 170 µm ,250 µm & 853 µm particles used in the present study calculations of Fig.1. It is evident that the Syamlal-O'Brien drag model predicts larger values of gas-solids exchange coefficient at a higher values of solids concentration. This means that the Syamlal and O'Brien drag model predictions are significant near the walls and drag coefficient will have the greatest influence on the model. Fig.1 shows the quantitative comparison of various drag models at fixed slip velocity of 0.5 m/s and for the 853µm particles used in the present study as part of validation. No significant difference between

drag coefficients predicted by the models at all values of solid volume fraction for the coarsest particles, i.e. 853 µm.

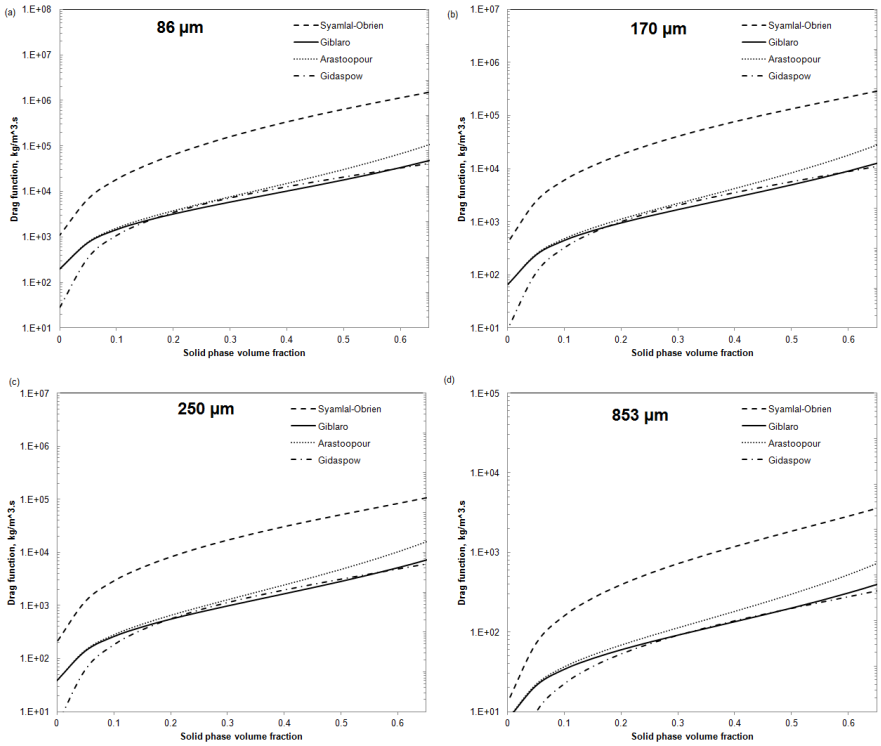

Fig. 1. Comparison of different drag models for (a) 86 µm particles (b) 170 µm particles (c) 250 µm particles (d) 853 µm particles at a slip velocity of 0.5 m/s.

3. Simulation strategy and conditions

This paper simulates two different fluidization geometries consist an internal draft tube. First geometry, 2D ICFB is considered from Ahuja & Patwardhan, (2008) work, used for validation of the CFD model. The second geometry, 3D ICFB from IITH's 30 cm diameter fluidization rig is used for parametric analysis. Ahuja & Patwardhan, (2008) experimented solid-gas flow patterns in ICFB with a small geometry (Column 0.186 m X 1.2 m with a draft tube of 0.10 m X 0.158 m) by considering a particular case as partial sparging with a draft tube, 2D simulations are performed using Eulerian–Eulerian two-fluid model along with No-slip boundary conditions were used for both phases at the ICFB walls. Solids volume fraction was defined as 0.62 with a maximum packing limit of 0.65. Simulation was initiated with uniform inlet superficial gas velocity of 1.041 m/s. In this work the 3D geometry of ICFB (0.3 mX 3.0 m & draft tube 0.1mX 0.9 m) height of draft tube as shown in Fig. 2(b). Grid consists of total 46536 nodes and two cell zones. The initial bed height as 0.86 m considered and the initial solid volume fraction was defined as 0.62 with a maximum packing of 0.65. Simulation was initiated with uniform inlet superficial gas velocity to the draft tube was set as 0.8, 1.25, 1.5 and 1.75 m/s with a constant uniform gas velocity of 0.2 m/s as an input to the annular section.

4. Results and discussion

4.1 2D ICFB model predictions & validation

In the current study, Gidaspow, Syamlal–O'Brien, Gibilaro and Arastoopour drag models are tested and compared with the experimental datato identify the suitable drag model for modelling the turbulent fluidization for gas-solid particles. This present work assumes two cases of experiments having partial and complete sparging for 2D ICFB CFD runs operating at a 1.0425 m/s superficial velocity.

Table 1

Simulation and model parameter

Parameter Description	**Value**
Particle density	2500 (kg/m^3)
Air density	1.225 (kg/m^3)
Mean particle diameter	86,170 and 250 (μm)
Initial solid packing	0.62
Superficial air velocity	0.8, 1.0, 1.25, 1.5, 1.75 (m/s)
Fluidized bed column dimension	0.3 (m) x 3.0 (m)
Static bed height	0.8 (m)
Restitution coefficient	0.95
Boundary Condition	Outlet- pressure, walls-No slip

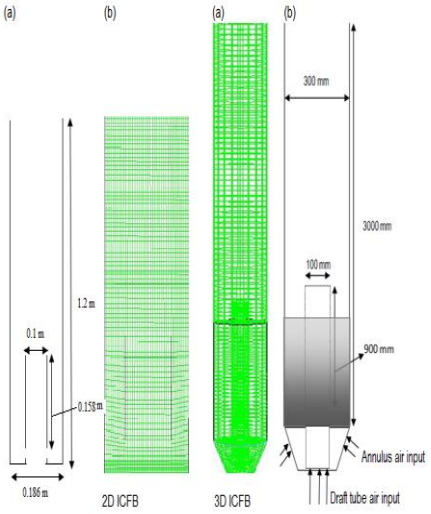

Fig. 2. Schematic diagrams of 2D ICFB (a) Geometry (b) Grid and 3D ICFB (a) Grid (b) Geometry.

The simulated results of the 2D ICFB are presented in Fig. 3-4 in terms of solid volume fraction and flow field. In Fig. 3, comparison between the various drag models based on solid volume fraction snapshot have made in terms of bed height and shape of fluidization pattern. It can be observed that the Arastoopour and Gidaspow drag models show the best results in simulating the bed height. The Gibilaro drag model prediction represents the lowest bed expansion and gas void fraction comparatively with other drag model predictions. The CFD models of Gidaspow, Syamlal-O'Brien and Arastoopour predict lean solids zone just above the gas distributor as seen in the Fig.3. Whereas in the case of Gibilaro drag model, predicts dense zone at the bottom of draft tube which is just above the gas distributor. In Fig.4 the predictions by Syamlal-O'Brien drag model based CFD model shows an improvement over the Gibilaro model.

4.2 Pressure drop in 3D ICFB

The mean Δp value is plotted to compare pressure difference at different locations along with 3D ICFB column as shown in the Fig. 5. The pressure drop in the draft tube passed through minima with an increase of gas superficial velocity. In the low velocity region the pressure drop decreases steadily. After minimum fluidization stage, once transport of solids moves upward then the pressure drop decreases with an increase of superficial velocity due to the lean solids holdup in the draft tube.

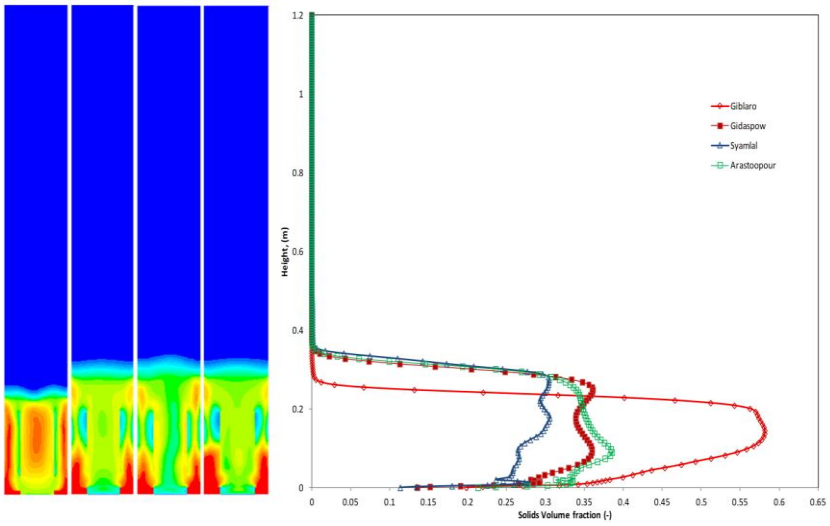

Fig. 3. The Simulated solid volume fraction contours for various drag models for partially sparging with a draft tube (Uo=1.0425 m/s) (a) Gibilaro drag model (b) Gidaspow drag model(c) Syamlal-O'Brien drag model and (d) Arastoopour drag model.

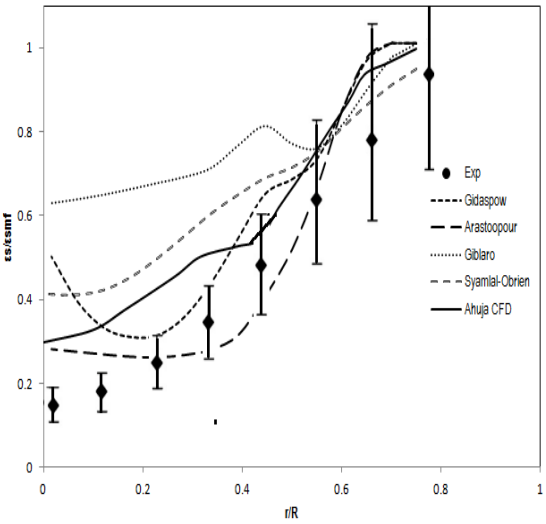

Fig. 4. Solids hold-up profiles for partial sparging with a draft tube: Comparison of different drag models of 853 µm particles.

The pressure drop at different heights of draft tube is following a decline trend with an increase of superficial gas velocity except at location of 0.25 m, which is just above the air distributor. At 0.25 m location, part of draft tube gas gets into by passing; the Δp seems unchanged at this gap area.

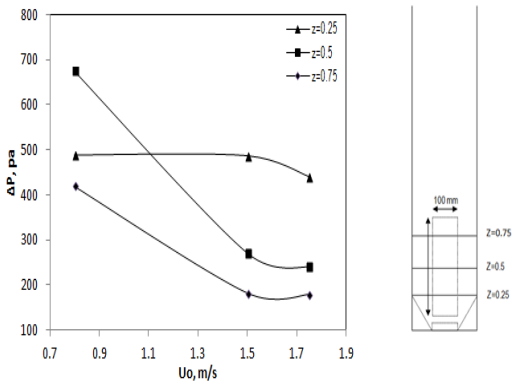

Fig. 5. Pressure drop vs draft tube veolcity for the silica particle size d_p=86 µm .

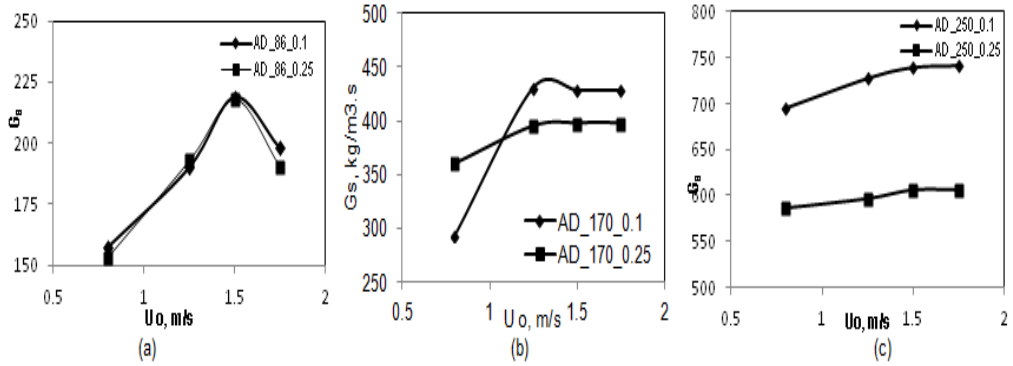

Fig. 6. Solids circulation rate vs draft tube velocity (a) 86 µm (b) 170 µm (c) 250 µm.

4.3 Solid Circulation Rate

Solid recirculation rate G_s is an important parameter to design 3D ICFB reactor with a suitable draft tube configuration. The effect of superfical gas velocity (U_o) on solid recirculation rate is shown in Fig. 6. Solids recirculation rate G_s was calculated based on the product of mean volume fraction of solids, density of solids and the solid velocity

magnitude. G_s increases with U_o due to the increase in the driving force for the circulation of solids between the draft tube and annular moving bed is observed through increased bed voidage in the draft tube. It can be seen in the Fig.6 (a), (b)and (c), that the solid curculation rate of smaller particles increases with the increase of superficial velocity.

4.4 Mean Volume fraction countor plots

Using the Arastoopour drag, contours of solid phase volume fractions are shown in Fig.7 ,10 & 11 for 86 µm 170 µm and 250 µm size silica particles at gas superficial velocities at 0.8, 1.25 and 1.5 m/s respectively. The bed expansion for different size particles is clearly distinguished from these contour plots. Fig. 7 is the simulation result of particle diameter 86µm size with the Arastoopour drag model. It is found that the bed expansion is low at low superficial gas velocities. There exist a dense phase zone in the lower part of the ICFB and a dilute phase zone in the upper zone. However the dense phase bed level increases gradually with increasing superficial gas velocity from 0.8 to 1.5 m/s. Similar behavior is also observed in the case of particles 170 µm and 250 µm as shown in the Fig. 8 & 9 respectively. In the case of 250 µm size particles as expected, due to the increase effective weight of the particles, the height of the bed expansion is lower compared to 170 and 86 µm particle profiles.

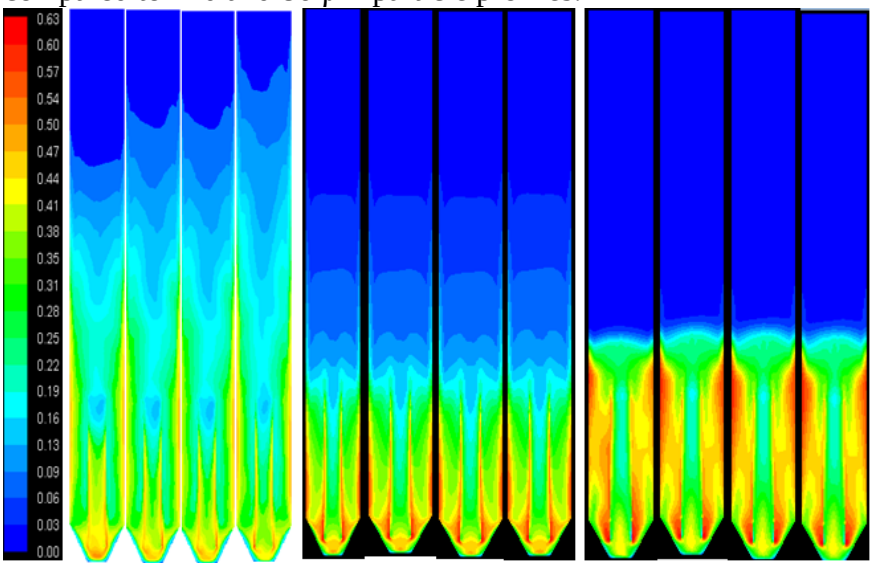

(a) (b) (c) (d) (a) (b) (c) (d) (a) (b) (c) (d)

Fig. 7. (a) Contour plot of solids volume fraction with different gas velocities of Silica particles of size 86 µm at a constant annulus input velocity (With Arastoopour drag model) U_a=0.2 m/s.(a) U_d=0.8 m/s (b) U_d=1.0 m/s (c) U_d=1.25 m/s (d) U_d=1.5 m/s.

Fig. 8. Contour plot of mean solids volume fraction with different gas velocities of Silica particles size 170 µm at constant annulus input velocity U_a=0.2 m/s (With Arastoopour drag model).(a) U_d=0.8 m/s.(b) U_d=1.25 m/s.(c) U_d=1.5 m/s.(d) U_d=1.75 m/s.

Fig. 11. Contour plot of mean solids volume fraction with different gas velocities of Silica particles size 250 µm at constant annulus input velocity U_a=0.2 m/s (With Arastoopour drag model). (a) U_d=0.8 m/s. (b) U_d=1.25 m/s. (c) U_d=1.5 m/s. (d) U_d=1.75 m/s.

5. Conclusion

The hydrodynamic characteristic of 2D & 3D ICFB with solid particle was studied by an Eulerian-Eulerian CFD model with the kinetic theory of granular flow. Four drag models considered for the simulations. Syamlal and O'Brien, Gidaspow, Arastoopour and Gibilaro drag models are implemented into Fluent through the User Defined Functions (UDF). 2D simulation of an internally circulating gas-solid fluidized bed with polypropylene particles was run based on Ahuja & Patwardhan, (2008) case. The resulting hydrodynamic properties are compared to Ahuja & Patwardhan, (2008) data. The simulation results by four different drag models show that the Gidaspow & Arastoopour models can accurately predict the flow pattern, voidage profiles, and velocity profiles in the ICFB. With the Arastoopour drag model the simulations are giving the best fits to the experimental data. The draft tube superficial gas velocity and the solids circulation rate have significant effects on the solid fraction in each region. Increasing the draft tube superficial gas velocity can decreases solid fraction in the draft tube but has little effect in the annulus zone.

6. References

Ahuja, G.N., & Patwardhan, A.W. (2008). CFD and experimental studies of solids hold-up distribution and circulation patterns in gas–solid fluidized beds. *Chemical Engineering Journal*, 143 147–160.

Arastoopour H., Pakdel, P., & Adewumi M. (1990) Hydrodynamic analysis of dilute gas–solids flow in a vertical pipe. *Powder Technology*, 62, 163–170.

Burugupalli, V.R. (1988). Process analysis of a twin fluidized bed biomass gasification system. *Industrial and Engineering Chemistry Research*, 27, 304–312.

Gibilaro, L.G., Di Felice, R., & Waldram, S.P. (1985). Generalized friction factor and drag coefficient correlations for fluid–particle interactions. *Chemical Engineering Science*, 40, 1817–1823.

Gidaspow, D. (1994). Multiphase flow and fluidization: Continuum and kinetic theory description. New York : Academic Press.

Gidaspow, D., Jonghwun, J., & Singh, R.K. (2004). Hydrodynamics of fluidization using kinetic theory: an emerging paradigm-2002 Flour–Daniel lecture. *Powder Technology*, 148, 123–141.

Gidaspow, D., & Mostofi,R. (2003). Maximumcarrying capacity and granular temperature of A, B, and C particles, *AIChE Journal*, 49, 831–843.

Jeon, J. H., & Kim, S.D (2010). Hydrodynamic Characteristics of Binary Solids Mixtures in aSquare Internally Circulating Fluidized Bed. *Journal of Chemical Engineering of Japan*, 43(2), 26-131.

Kim, Y.T., Song, B.H., & Kim, S.D. (1997). Entrainment of solids in an internally circulating fluidized bed with draft tube. *Chemical Engineering Journal*, 66, 105-110.

Kim, Y.J., J.M. Lee and S.D. Kim, (2000). Modeling of Coal Gasification in an Internally Circulating Fluidized Bed Reactor with Draught Tube. *Fuel*, 79**,** 69-77.

Lun, C.K.K., Savage, S.B., Jeffrey, D.J., and Chepurniy,N. (1984). Kinetic theories for granular flow: inelastic particles in Couette flow and slightly inelastic particles in a general flow field. *Journal of Fluid Mechanics*, 140, 223–256.

Mujumdar, A.S., & Wu, Z. (2008). Thermal drying technologies Cost-effective innovation aided by mathematical modeling approach. *Drying Technology*, 26, 146–154.

Patankar, S.V. (1980). Numerical Heat Transfer and Fluid Flow. Hemisphere Publishing Corporation.

Syamlal, M., Rogers, W., & O'Brien., T.J. (1993). MFIX documentation: theory guide, Technical Report DOE/METC-9411004, NTIS/(DE9400087) Morgantown Energy Technology Centre, Morgantown, West Virginia.

Syamlal, M & O'Brien, T.J. (1989). Computer simulation of bubbles in a fluidized bed. *AIChE Symposium Series*, 85, 22–31.

Van Wachem, B.G.M., Schouten, J.C., Krishna, R., Van den Bleek, C.M., & Sinclair, J. L. (2001). Comparative analysis of CFD models of dense gas–solid systems," *AIChE Journal*, 47,1035–1051.

Wen, Y.H., & Yu. (1966). Mechanics of fluidization.*Chemical Engineering Progress Symposium Series*, 62, 100–111.

Yang, W.C., & Keairns, D.L. (1978). Design of recirculating fluidized beds for commercial applications. *AIChE Symposium Series*, 74, 218–228.

Yang, T., Zhang, T., & Bi, H. T. (2008). A novel continuous reactor for catalytic reduction of NOx – Fixed bed simulation. *The Canadian Journal of Chemical Engineering*, 86(3), 395-402.